Aust. J. Phys., 1974, **27**, 837–53

Measurements of Ionospheric Refraction at 80 MHz Using Discrete Radio Sources

O. B. Slee and P. Y. Lee

Division of Radiophysics, CSIRO, P.O. Box 76, Epping, N.S.W. 2121.

Abstract

About 2000 measurements of source positions obtained at 80 MHz with the Culgoora radioheliograph near the peak of the solar activity cycle in 1968–71 have been used to determine the regular ionospheric refraction. Diurnal, seasonal and zenith-angle dependencies of the refraction are deduced and found to be qualitatively consistent with the known gradients in peak electron density. The variability of the refraction from one measurement to the next is found to depend upon the zenith angle and season and to be mainly due to ionospheric disturbances whose presence is not usually revealed by measurements of the F_2 critical frequency. A quantitative comparison of the measured values of angular refraction with the F_2 critical frequency and its north–south and east–west gradients demonstrates the validity of the theoretical expressions for regular refraction developed by Komesaroff (1960) and yields a value of 190 ± 12 km for the equivalent thickness of the nocturnal ionosphere. A comparison of the present measurement of the thickness parameter with measurements of the same quantity made during the minimum of solar activity shows that the shape of the F_2 layer is not dependent on the solar activity cycle and hence is not a sensitive measure of the gas temperature.

1. Introduction

Measurements of the total ionospheric refraction of rays from discrete radio sources have been restricted in the past because of the lack of sufficient angular resolution at the lower radio frequencies where the ionosphere is most strongly refracting. Payne-Scott and McCready (1948) made some exploratory measurements of ionospheric refraction on solar radio sources using a sea-interferometer. The first reported measurements of ionospheric refraction using cosmic radio sources were made by Smith (1952). He showed that the variations in apparent right ascension of four radio sources at 81·5 MHz were consistent with the average east–west gradients in the F_2 critical frequency over south-east England if certain assumptions were made about the radial distribution of electron density. In order to account for the observed magnitude of the refraction, the columnar electron content above the level of maximum ionization needed to exceed that below the F_2 maximum by a considerable factor; this deduction has since been verified by lunar–radar and satellite measurements.

Komesaroff (1960) developed a theory for refraction by horizontal gradients in ionization in the F region and showed that the angular deviations which he observed in radio source positions at 19·7 MHz agreed with his theory. However, his observations were limited to relatively few measurements on two sources within 20° of the zenith and he did not discuss the important influence on his measurements of the irregular component of ionospheric refraction due to ionospheric disturbances.

Between October 1967 and December 1971, Slee and Higgins (1973) used the radioheliograph, operated by the Division of Radiophysics, CSIRO, at Culgoora, N.S.W., to measure the positions and flux densities of 777 radio sources. Many of these sources have accurate high-frequency radio positions, which are not significantly influenced by ionospheric refraction. Therefore the difference between the radioheliograph position (which can be measured to about 10″ arc for the stronger sources) and the high-frequency radio position can yield the ionospheric refraction at the time of the 80 MHz measurement.

The observing technique and method of reducing the observations to yield the angular refraction are described in Section 2. In Section 3 about 2000 measurements of positions at 80 MHz are used to find the average dependence of the regular ionospheric refraction on zenith angle, local time and season. The 80 MHz measurements were confined to the nocturnal interval 16^h to 08^h local time. The dependence of the irregular component of ionospheric refraction on zenith angle, local time and season is discussed in Section 4. Section 5 is concerned with the relationship between the measured 80 MHz refraction and the ionospheric critical frequencies at various locations in Australasia. The equations for the theoretical treatment of refraction given by Komesaroff (1960) are used to separate the components of regular refraction due to horizontal and radial gradients in ionospheric electron density and to derive the 'equivalent thickness' of the ionosphere during this period near sunspot maximum. Section 6 explores the dependence of the thickness parameter on solar activity and compares the present measurements with those made at similar latitudes using satellite transmissions.

2. Observations and Reductions

The method of observing sources has been discussed in detail by Slee and Higgins (1973). Briefly, the source under observation was straddled in declination by eight of the heliograph's radio beams, each about $3'{\cdot}7$ arc to half-power points and separated by $\sim 2'{\cdot}1$ arc in declination. About 10 drift scans, each 64 s in duration, were later averaged and the centroids of the profiles in both hour angle and declination were measured to give the apparent position of the source. This method of observation and subsequent reduction averages out most of the small angular deviations associated with ionospheric scintillations, which have quasi-periods <60 s. The slower position changes associated with ionospheric disturbances are not greatly reduced in amplitude by smoothing over ~ 10 min.

The measured coordinates of each source were precessed to epoch $1950{\cdot}0$ and, together with the date and hour angle at the centre of the observation, were written on a magnetic tape. A subsequent computer operation compared the precessed coordinates with the accurate high-frequency radio coordinates and wrote the position differences, together with the date and local time of the observation, on another magnetic tape. Additional computer programs sorted the refraction measurements to investigate dependences on zenith angle, local time and season.

The source observations were made within 1 h of local transit and covered the complete declination range of the radioheliograph from $+35°$ to $-45°$. Each observing session lasted for about seven consecutive nights, observations beginning

at $\sim 16^h$ and ending the following morning at $\sim 08^h$; 14 observing sessions were used to provide the data for the present analysis and the sessions were fairly evenly divided between the seasons.

Although it may appear that the heliograph positions should be corrected for tropospheric refraction before the ionospheric refraction can be isolated, it can be shown that any aerial system which relies on the combination of spaced elements to form the radio image will, to a first-order approximation, automatically compensate for tropospheric refraction if the element spacings used for computing the angular position of the aerial beam are expressed in free-space wavelengths. This result depends upon the fact that the bending of the incoming rays in an assumed horizontally stratified troposphere is exactly cancelled out by the effect of the ground-level refractive index on the measured signal phase. In the case of the radioheliograph, where the element spacing of 3 km does not strictly allow the assumption of a plane stratified troposphere, a small correction for tropospheric refraction should be applied; however, the correction is always less than 1″ arc, and it has been neglected in the present analysis.

3. Observed Refraction

Angular refraction may be expected to show dependence on local time, season and zenith angle. In addition, the refraction should not be expected to show exactly the same properties in hour angle and declination. Since the measurements were made near source transit, the refraction in declination is equivalent to almost a pure change in zenith angle in the north–south direction. The observed refraction in declination, $\Delta\delta \equiv (\Delta\delta)_w + (\Delta\delta)_s$, consists of two well-defined components: the wedge component $(\Delta\delta)_w$ due to the north–south gradient in total electron content, and the spherical component $(\Delta\delta)_s$ due to the radial gradient in ionization. The wedge component shifts the apparent position of the source towards the direction of increasing total electron content while the spherical component shifts the source towards the zenith. On the other hand, the observed refraction in hour angle ΔH contains practically no component due to spherical refraction; thus $\Delta H \equiv (\Delta H)_w$ reflects only the influence of the east–west gradient in electron content.

The complex dependences of angular refraction on ionospheric properties and the differences between $\Delta\delta$ and ΔH make refraction a difficult quantity to portray in any one plot or table. In the present analysis the measurements of $\Delta\delta$ and ΔH are presented separately in three tables and three plots showing their dependences on season, local time and zenith angle. The standard deviation associated with each measurement is also tabulated, together with the number of observations, allowing the internal standard errors in $\Delta\delta$ and ΔH to be estimated.

Hour Angle Refraction ΔH

The experimental results for ΔH are listed in Tables 1*a*–1*c* and plotted in Figs 1*a*–1*c* to show the dependence of ΔH on zenith angle, season and local time. The values of ΔH shown in these tables and plots were obtained by averaging the ΔH from N sources contained within 20° zones of declination (zenith angle Z), 4 h intervals of local time and three monthly seasons. For example, in Table 1*a* and Fig. 1*a* the entry (summer, $Z = 35°$) is the average value of ΔH from all sources in the declination

zone $-5° < \delta < 15°$ ($25° < Z < 45°$) recorded at all nocturnal hours during the months of November, December and January. Thus the averaging is performed over the complete range of the parameter not appearing in the particular table or plot, and three tables and plots are required to describe the observations fully. Inspection of the standard deviations $(\Delta H)_{\rm rms}$ and the number of observations which have been averaged to obtain each value shows that the typical internal standard error associated with each point is $\sim 0'\cdot 1$.

Table 1. Dependence of ΔH on zenith angle, season and local time

(a) ΔH as a function of zenith angle and season

Season	$Z = 50°$			$Z = 35°$			$Z = 15°$			$Z = -5°$		
	N	ΔH	$(\Delta H)_{\rm rms}$	N	ΔH	$(\Delta H)_{\rm rms}$	N	ΔH	$(\Delta H)_{\rm rms}$	N	ΔH	$(\Delta H)_{\rm rms}$
Summer	79	−0′·66	1′·86	187	−0′·38	1′·42	95	−0′·41	1′·14	73	−0′·07	0′·94
Autumn	108	−0·31	1·28	144	+0·32	1·07	102	−0·02	1·07	85	+0·02	0·70
Winter	115	+0·02	1·30	217	0·00	1·11	185	−0·06	1·14	124	+0·10	0·87
Spring	53	−0·22	1·80	122	−0·09	1·18	92	+0·08	0·93	57	+0·09	0·77
All seasons	355	−0·27	1·53	670	−0·05	1·23	474	−0·10	1·10	339	+0·04	0·83

(b) ΔH as a function of season and local time

Local time	Summer			Autumn			Winter			Spring		
	N	ΔH	$(\Delta H)_{\rm rms}$	N	ΔH	$(\Delta H)_{\rm rms}$	N	ΔH	$(\Delta H)_{\rm rms}$	N	ΔH	$(\Delta H)_{\rm rms}$
$17^{\rm h}$	60	−0′·12	1′·39	62	+0′·07	1′·22	87	+0′·67	0′·93	23	+0′·50	1′·60
$20^{\rm h}$	104	−0·33	1·37	129	+0·41	1·10	158	+0·21	1·02	47	−0·31	1·34
$00^{\rm h}$	88	−0·36	1·57	105	−0·08	0·99	150	−0·17	1·04	93	+0·22	1·03
$04^{\rm h}$	130	−0·46	1·39	118	−0·06	0·90	156	+0·03	1·10	119	+0·12	0·89
$07^{\rm h}$	52	−0·63	0·85	25	−1·12	1·07	90	−0·74	1·10	42	−0·93	1·40
All times	434	−0·38	1·40	439	+0·03	1·09	641	+0·01	1·11	324	−0·03	1·18

(c) ΔH as a function of zenith angle and local time

Local time	$Z = 50°$			$Z = 35°$			$Z = 15°$			$Z = -5°$		
	N	ΔH	$(\Delta H)_{\rm rms}$	N	ΔH	$(\Delta H)_{\rm rms}$	N	ΔH	$(\Delta H)_{\rm rms}$	N	ΔH	$(\Delta H)_{\rm rms}$
$17^{\rm h}$	37	+0·12	1′·79	89	+0′·34	1′·30	62	+0′·32	1′·08	42	+0′·32	0′·68
$20^{\rm h}$	86	−0·17	1·40	179	+0·18	1·20	96	+0·05	1·20	77	+0·18	0·94
$00^{\rm h}$	82	−0·15	1·69	129	−0·09	1·14	136	−0·11	1·01	89	−0·08	0·78
$04^{\rm h}$	104	−0·26	1·45	188	−0·08	1·15	122	−0·04	1·01	109	−0·01	0·72
$07^{\rm h}$	46	−0·95	0·95	85	−0·85	1·21	58	−0·84	1·00	22	−0·20	1·12
All times	355	−0·27	1·53	670	−0·05	1·23	474	−0·10	1·10	339	+0·04	0·83

The main feature of Fig. 1*a* is the significant difference between summer and the other three seasons as far as the dependence of refraction on zenith angle is concerned. Since ΔH is dominated by the wedge component of refraction it is clear that in summer there is, on average, a well-defined east–west gradient in total electron content with the ionization increasing to the east. The easterly refraction increases steadily with increasing zenith angle, but it is shown later that this behaviour is consistent with a reasonably constant value of east–west ionization gradient in the ionosphere over the latitude range 31° S. to 25° S. included in this range of zenith angles.

Fig. 1*b* shows how ΔH varies with local time for each season. Again, summer is seen to be markedly different from the other seasons. In summer the west to east gradient in ionization noted in Fig. 1*a* is well defined at all hours of the late afternoon and night and in the early morning, when it tends to reach its highest value. During the other seasons, the sources are refracted towards the west during the late afternoon

and early evening and then suffer little refraction for most of the night until near local dawn, when a strong gradient in ionization is established with total electron content increasing towards the east.

Fig. 1*c* shows the dependence of ΔH on local time for various zenith angles. The plots have similar shapes, which show the sources to be refracted towards the

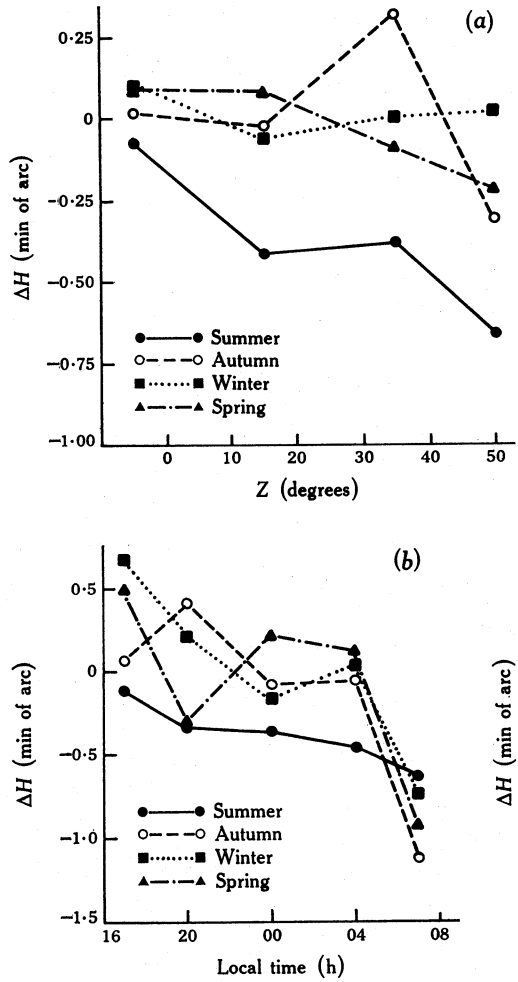

Fig. 1. Plots of refraction in hour angle ΔH as a function of:

(*a*) zenith angle Z for each season,

(*b*) local time for each season,

(*c*) local time for each range of Z.

Each point represents the average of 100–200 separate measurements of refraction; the internal standard error associated with each point is typically 0′·1 arc (see Table 1 for details). Positive values of ΔH indicate refraction to the west.

west in the late afternoon and early evening and then to change to a modest easterly deviation which remains fairly constant for much of the night; just before local dawn the west to east gradient increases rapidly.

Much of the behaviour shown by the experimentally measured values of ΔH can be attributed to the well-known gradients in ionospheric ionization that have been established by ionospheric sounding. For example, strong east–west gradients in critical frequency are usually measured near local dawn and sunset, accounting for the marked westerly refraction near sunset and the strong easterly deviation near dawn.

The persistent easterly increase in ionization on summer nights noted in Figs 1*a* and 1*b* appears to be inconsistent with the known behaviour of the nocturnal ionosphere. However, it is well known (see e.g. Ratcliffe and Weekes 1960) that contours of maximum electron density in the F_2 region tend to lie parallel to the geomagnetic equator rather than to the geographic equator. Thus at times other

Table 2. Dependence of $\Delta\delta$ on zenith angle, season and local time

(a) $\Delta\delta$ as a function of zenith angle and season

Season	$Z = 50°$			$Z = 35°$			$Z = 15°$			$Z = -5°$		
	N	$\Delta\delta$	$(\Delta\delta)_{rms}$	N	$\Delta\delta$	$(\Delta\delta)_{rms}$	N	$\Delta\delta$	$(\Delta\delta)_{rms}$	N	$\Delta\delta$	$(\Delta\delta)_{rms}$
Summer	79	+0′·87	2′·74	187	+0′·77	1′·76	95	+0′·84	1′·40	73	+0′·86	1′·28
Autumn	108	−0·10	1·53	144	+0·35	1·22	102	+0·45	1·16	85	+0·44	0·66
Winter	115	+0·09	1·51	217	+0·33	1·46	185	+0·48	0·92	124	+0·57	0·77
Spring	53	−0·38	1·68	122	+0·03	1·25	92	+0·35	0·96	57	+0·46	1·04
All seasons	355	+0·13	1·92	670	+0·40	1·49	474	+0·52	1·10	339	+0·58	0·94

(b) $\Delta\delta$ as a function of season and local time

Local time	Summer			Autumn			Winter			Spring		
	N	$\Delta\delta$	$(\Delta\delta)_{rms}$	N	$\Delta\delta$	$(\Delta\delta)_{rms}$	N	$\Delta\delta$	$(\Delta\delta)_{rms}$	N	$\Delta\delta$	$(\Delta\delta)_{rms}$
17^h	60	+1′·56	1′·65	62	+0′·91	1′·58	87	+0′·31	0′·92	23	−0′·19	1′·40
20^h	104	+0·74	2·06	129	+0·15	0·86	158	+0·36	1·36	47	+0·17	1·42
00^h	88	+1·01	1·63	105	+0·55	1·16	150	+0·31	1·12	93	+0·39	1·36
04^h	130	+0·47	1·52	118	−0·13	1·13	156	+0·42	1·40	119	−0·23	1·01
07^h	52	+0·28	1·93	25	+0·18	1·66	90	+0·52	1·11	42	+0·60	1·10
All times	434	+0·82	1·84	439	+0·28	1·23	641	+0·38	1·23	324	+0·13	1·25

(c) $\Delta\delta$ as a function of zenith angle and local time

Local time	$Z = 50°$			$Z = 35°$			$Z = 15°$			$Z = -5°$		
	N	$\Delta\delta$	$(\Delta\delta)_{rms}$	N	$\Delta\delta$	$(\Delta\delta)_{rms}$	N	$\Delta\delta$	$(\Delta\delta)_{rms}$	N	$\Delta\delta$	$(\Delta\delta)_{rms}$
17^h	37	+0′·19	1′·44	89	+0′·71	1′·62	62	+1′·06	1′·17	42	+0′·78	1′·46
20^h	86	+0·27	2·18	179	+0·28	1·47	96	+0·44	1·09	77	+0·59	0·61
00^h	82	+0·37	2·01	129	+0·46	1·35	136	+0·60	0·98	89	+0·66	0·87
04^h	104	−0·25	1·33	188	+0·25	1·60	122	+0·13	1·08	109	+0·43	0·91
07^h	46	−0·12	2·07	85	+0·47	1·20	58	+0·75	1·12	22	+0·64	0·98
All times	355	+0·13	1·92	670	+0·40	1·49	474	+0·52	1·10	339	+0·58	0·94

than near local sunset and dawn the maximum ionization gradient in eastern Australia should be directed towards the north–north-east. The component of this vector resolved in the east–west direction is responsible for the observed ΔH; in summer, when the ionization gradient is highest, the resolved component may have sufficient magnitude to result in detectable easterly refraction through most of the night.

We shall make a detailed comparison between the measured refraction and ionospheric critical frequencies in Section 5. Here it is sufficient to point out that the measured summer values of the east–west gradient in maximum electron density (shown as triangles in Fig. 5) are all directed towards the east and are of a magnitude to account for the observed easterly refraction. The inclination of the maximum ionization gradient to geographical north can be obtained either from the measurements of critical frequency or from the ratio of the refraction components $(\Delta H)_w/(\Delta\delta)_w$. Leaving out the measurements near dawn and sunset, we find that the summer data plotted in Figs 5 and 6 give average inclinations of 21° E. and 15° E. from the ionosonde and refraction measurements respectively. This compares satisfactorily with the magnetic declination at Culgoora of ~12° E.

Declination Refraction $\Delta\delta$

The experimental results for 80 MHz refraction in declination are listed in Tables 2*a*–2*c* and plotted in Figs 2*a*–2*c*. The averaging procedure is identical with that employed in presenting the results for ΔH. In interpreting these results it should be remembered that $\Delta\delta$ is formed by the addition of a wedge component $(\Delta\delta)_w$ and

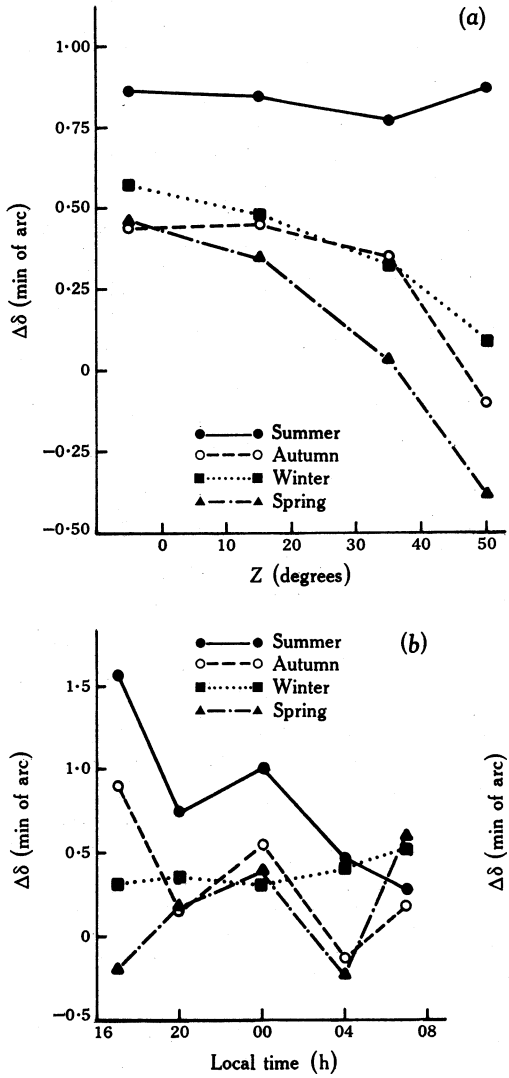

Fig. 2. Plots of refraction in declination $\Delta\delta$ as a function of:

(*a*) zenith angle Z for each season,

(*b*) local time for each season,

(*c*) local time for each range of Z.

Each point represents the average of 100–200 separate measurements of refraction; the internal standard error associated with each point is typically 0′·1 arc (see Table 2 for details). Positive values of $\Delta\delta$ indicate refraction to the north.

a spherical component $(\Delta\delta)_s$. It is known from world-wide ionospheric soundings that the north–south gradients are usually positive towards the equator; thus in these results the wedge component of refraction will usually shift the source to the north. The spherical component, which is significant only at the larger zenith angles, always shifts the source towards the zenith; in these results the spherical component will thus shift the declination to the south.

Fig. 2*a* shows the dependence of $\Delta\delta$ on zenith angle for each season (Fig. 1*a* shows the equivalent results for ΔH). It is clear that the plot for summer is significantly different in form from those of the other seasons. The shapes of these curves are plausibly explained by considering the relative contributions of the wedge and spherical components of refraction as functions of season and zenith angle. For all seasons except summer the northerly refraction decreases steadily with increasing zenith angle, reflecting the increasing contribution made to the total refraction by the spherical refraction at the larger zenith angles. In summer the north–south gradient in ionization remains high on most nights, with the result that the wedge component is strong relative to the spherical component; this maintains the net refraction well to the north even at the largest zenith angles.

Fig. 2*b* shows how $\Delta\delta$ varies with local time for each season. It is clear that in summer the deviation is always to the north, being greatest in the late afternoon and least about local dawn; a subsidiary maximum occurs about local midnight. The generally high values of $\Delta\delta$ in summer reflect the higher north–south gradients in ionization during this season. Autumn shows a curve similar in form to that of summer but the values of $\Delta\delta$ are generally lower and the sign of the north–south gradient can actually reverse when the critical frequency is lowest just before local dawn. In winter $\Delta\delta$ maintains a uniformly low value over the night, while in spring the summer and autumn variation reappears, with the notable difference that the north–south gradient on a late spring afternoon seems particularly low or even reversed.

Fig. 2*c* shows the dependence of $\Delta\delta$ on local time for various zenith angles. It is clear that the dependence of $\Delta\delta$ on local time is of similar form for all zenith angles but there is a systematic displacement between the curves. The net refraction is generally towards the north with minima near 20^h and 04^h. The magnitude of the northerly displacement is reduced as the zenith angle increases, showing the influence of the rising contribution to the total refraction from the spherical component.

4. Irregular Component of Refraction

Each of the average values of refraction listed in Tables 1 and 2 is associated with a standard deviation $(\Delta\delta)_{rms}$ and $(\Delta H)_{rms}$ which is a measure of the variation in the apparent source position due to a number of factors. The system noise fluctuation level is not an important contributor to the standard deviation; an analysis of the position measurements on a number of calibrator sources, which were each observed many times by Slee and Higgins (1973), showed that the dispersion about the mean position was not related to the signal to noise ratio of the particular source, as would be expected if noise were affecting the position measurements. The influence of ionospheric scintillation is also expected to be unimportant, because each position is obtained by averaging over 10 min, which is much longer than the duration of a typical scintillation. This conclusion is supported by the entries for $(\Delta H)_{rms}$ and $(\Delta\delta)_{rms}$ in Tables 1*b*, 1*c*, 2*b* and 2*c* which do not show the marked increase near local midnight (see e.g. Smerd and Slee 1966) that is characteristic of the diurnal incidence of ionospheric scintillations.

The most important contributors to the variance are likely to be the influence of ionospheric disturbances and the normal variability in the regular refraction due to changes in ionization from day to day.

An inspection of Tables 1 and 2 is sufficient to show that $(\Delta H)_{\text{rms}}$ and $(\Delta\delta)_{\text{rms}}$ are not strongly dependent on local time; they depend strongly, however, on the zenith angle and to a lesser extent on the season. Figs 3*a* and 3*b* show more clearly the dependence of $(\Delta H)_{\text{rms}}$ and $(\Delta\delta)_{\text{rms}}$ on season and zenith angle. Both $(\Delta H)_{\text{rms}}$ and $(\Delta\delta)_{\text{rms}}$ increase systematically with increasing zenith angle. The increase by a factor of about two during all seasons over the zenith-angle range 0° to 60° strongly suggests that the irregular component of refraction is proportional to the secant of the zenith angle, or in other words is proportional to the path length of the ray

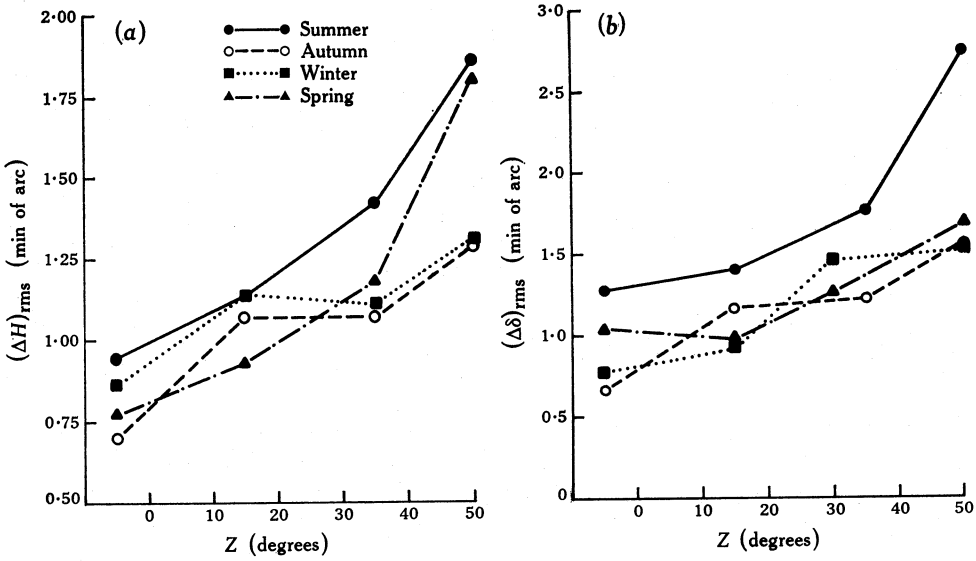

Fig. 3. Plots of the standard deviations $(\Delta H)_{\text{rms}}$ and $(\Delta\delta)_{\text{rms}}$ of the mean values of ΔH and $\Delta\delta$ showing their dependence on zenith angle Z for each season. Further information is contained in Tables 1 and 2.

through the ionosphere. It is clear that the irregular component is strongest on summer nights, especially the north–south or declination component; the declination component is also on average rather stronger than the hour angle component.

It is of interest to break down the total variances represented by $(\Delta H)_{\text{rms}}$ and $(\Delta\delta)_{\text{rms}}$ into what are believed to be their two main components: the variance due to the day-to-day variation in total ionization, and the variance due to the effects of ionospheric disturbances. Six of the strongest radio sources used in the present analysis were each observed on $\sim$30 separate occasions under widely different ionospheric conditions. With the theoretical expressions for refraction given by Komesaroff (1960) and the measured ionospheric critical frequencies at a network of sounders in Australasia, the total refraction was calculated for each of the 30 observations of the six radio sources. (The justification for using the theoretical expressions is given in Section 5.) The variance of the mean of the calculated value of refraction for each source was compared with the variance of the mean of the observed values of refraction. The results of these calculations and comparisons are given in Table 3.

It is clear from Table 3 that if the variance due to ionospheric disturbances is assumed to be the difference between the observed and calculated variances then the ionospheric disturbances are responsible for most of the irregular component of

refraction; on the average its contribution to the total variability is a factor of two greater than that of the normal day-to-day variation in peak electron content as measured by the ionospheric sounders. Under these circumstances the regular measurement of radio source positions throughout the day by means of the radio-heliograph may be a powerful method of detecting the passage of ionospheric density waves. Such measurements are currently in progress and will be reported in a later paper.

Table 3. Comparison between theoretical and observed variances for six well-observed radio sources

Source CUL No.	No. of observations	Standard deviation in mean $\Delta\delta$ Computed	Observed	Ionos. disturb.[A]
0218−02	22	0′·70	1′·72	1′·57
0331−01	22	0 ·55	1 ·03	0 ·87
0710+11	34	0 ·81	1 ·54	1 ·32
0812−02	26	0 ·39	0 ·97	0 ·89
1420+19	35	0 ·63	1 ·35	1 ·20
2045+06	28	0 ·72	1 ·33	1 ·12

[A] The variance due to ionospheric disturbances is assumed to be the difference between the observed and computed variances.

5. Correlation between 80 MHz Refraction and Measured Ionospheric Parameters

The statistical results described in Section 3 show well-defined dependences on season, zenith angle and local time. This suggests that a comparison between the 80 MHz measurements of refraction and ionospheric parameters such as critical frequency and ionization gradient, as determined by a network of Australasian ionospheric sounders, may prove fruitful. Such a comparison may confirm the validity of the theoretical treatment of refraction and consequently permit the determination of the total columnar electron content of the F_2 layer. Before the experimental results are presented, however, it is pertinent to consider the equations obtained by Komesaroff (1960) in his theoretical treatment of radio source refraction.

Komesaroff's (1960) analysis is valid for observations near transit and zenith angles $<60°$. The development of the theory does not depend upon any particular model for the shape of the radial electron density profile, provided it is unimodal and falls off reasonably quickly above the level of maximum ionization. At a frequency of 80 MHz ($\sim$10 times the F_2 critical frequency) Komesaroff's equations may be further simplified without significant loss of accuracy to the equations given below. The expression for $\Delta\delta$, the refraction in declination, consists of the sum of two well-defined components:

$$\Delta\delta = (\Delta\delta)_w + (\Delta\delta)_s , \tag{1}$$

with

$$(\Delta\delta)_w = \frac{9{\cdot}85\times10^4\,\tau\sec^2 Z}{(r_b+3\tau/2)f^2}\frac{\partial(f_c^2)}{\partial\phi}, \tag{2}$$

$$(\Delta\delta)_s = \frac{1{\cdot}72\times10^3\,\tau\sec^2 Z\tan Z}{r_m}\left(\frac{f_c}{f}\right)^2, \tag{3}$$

where $(\Delta\delta)_w$ and $(\Delta\delta)_s$ are the wedge and spherical components of refraction in minutes of arc, Z is the zenith angle of the source in degrees, f_c is the critical frequency of the F_2 layer in megahertz, f is the observing frequency in megahertz, r_b is the radius of the lower ionospheric bounding surface in kilometres, r_m is the radius of the surface of maximum electron density in kilometres, $\partial(f_c^2)/\partial\phi$ is the north–south gradient in the square of the critical frequency in MHz^2 per degree of latitude, and τ, the equivalent thickness of the ionosphere in kilometres, is defined by the equation

$$\tau N_m = \int N(r)\,dr, \tag{4}$$

in which $N(r)$ is the radial distribution of electron density (cm^{-3}) and N_m is the electron density at the radius of maximum ionization. Thus τ can be interpreted as the thickness of a hypothetical layer with everywhere the maximum electron density and the same total columnar electron content as the true F_2 region. It is therefore an important quantity which can be determined from observations of refraction.

The equation for the refraction in hour angle is

$$\Delta H \equiv (\Delta H)_w = \frac{9{\cdot}85\times10^4\,\tau\sec\phi_a\sec\delta\sec Z}{(r_b+3\tau/2)f^2}\,\frac{\partial(f_c^2)}{\partial L}, \tag{5}$$

where the symbols and units are as for equation (2) with the addition that ϕ_a is the latitude of the point at which the ray intersects the upper ionospheric boundary, δ is the declination of the source, and $\partial(f_c^2)/\partial L$ is the east–west gradient in the square of the critical frequency in MHz^2 per degree of longitude. The values adopted for r_b, r_m and the radius of the upper ionospheric boundary (which determines ϕ_a) are not critical; for example, an error of 100 km in r_b or r_m will produce an error of $1{\cdot}5\%$ in the calculated refraction, while a change of 200 km in the radius of the upper ionospheric boundary will result in a 2% change in ΔH. We have adopted the following heights for the various boundaries: lower ionospheric boundary at 230 km, maximum electron density at 350 km and upper ionospheric boundary at 600 km.

We have already shown from the discussion of Table 3 in Section 4 that most of the day-to-day variations in refraction are due to ionospheric disturbances, which do not significantly influence ionosonde measurements of critical frequency. In order to reduce the irregular component to a level well below that which we believe can be predicted by the ionosonde observations, we averaged ~30 individual measurements and compared this average with the corresponding ionospheric parameter obtained by averaging the hourly values which were observed during the time interval occupied by the radio observations. To achieve this in the present analysis the radio observations were considered session by session, and the measurements made during each of the 14 sessions were subdivided into five 4-h intervals of local time and four 20° zones of declination (zenith angle). Thus, for example, a pair of averaged measurements $\langle\Delta H\rangle,\langle\Delta\delta\rangle$ obtained in one session from all the sources observed during local times 00^h to 04^h in the declination range 15° to 35° would be compared with the ionospheric hourly soundings averaged over the local time interval 00^h to 04^h on the same days occupied by that particular observing session. The critical frequencies recorded by ionospheric sounders at Townsville, Brisbane, Canberra, Norfolk Island, Salisbury and Woomera were used in the comparison.

The latitude of Culgoora (30° 18′ S.) and the fact that the sources were observed within an hour of transit ensured that the rays passed through the F_2 region within a few hundred kilometres of Brisbane. Thus the measurement of $[f_c]_B$, the critical frequency at Brisbane, has been used in equation (3) for the calculation of $(\Delta\delta)_s$. The differences in f_c^2 between Townsville, Brisbane and Canberra have been used to estimate the value of $[\partial(f_c^2)/\partial\phi]_B$, the north–south gradient in f_c^2 at Brisbane. Similarly, the differences in f_c^2 between Norfolk Island, Brisbane and Salisbury or Woomera give an estimate of $[\partial(f_c^2)/\partial L]_B$, the east–west gradient of f_c^2 at Brisbane. However, before estimating the east–west gradient, it was first necessary to correct the recorded critical frequencies at Norfolk Island, Salisbury and Woomera for their different latitudes using the north–south gradient between Brisbane and Canberra.

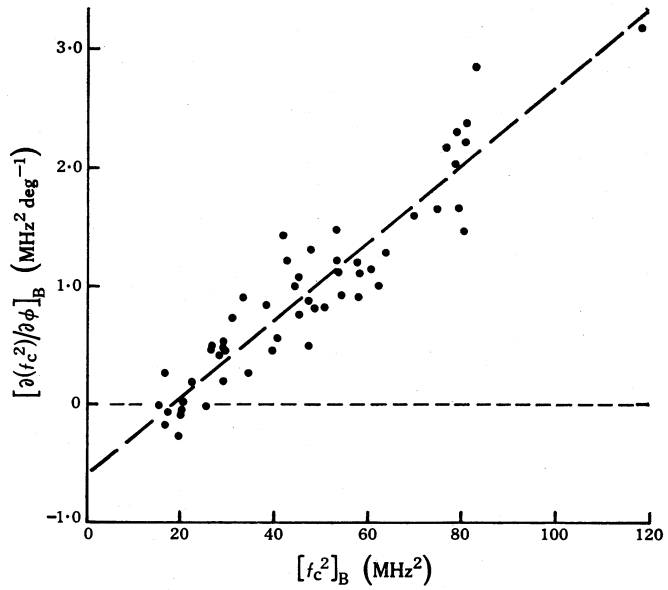

Fig. 4. Correlation diagram showing the dependence of the north–south gradient of the square of the critical frequency on f_c^2 at Brisbane. Positive values of $\partial(f_c^2)/\partial\phi$ indicate electron density increase towards the north.

During the course of this analysis it was found that one or other of the ionospheric sounders along the 150° meridian of longitude was sometimes not operating for a significant part of the observing session. A satisfactory estimate of $[\partial(f_c^2)/\partial\phi]_B$ could be made in these cases from the critical frequency at Brisbane using the following method. A plot of $[f_c^2]_B$ against $[\partial(f_c^2)/\partial\phi]_B$ on the occasions for which all the ionospheric sounders were operating showed a well-defined relationship, which is reproduced in Fig. 4. The plot shows that, to a fair degree of accuracy, $[\partial(f_c^2)/\partial\phi]_B$ increases linearly with $[f_c^2]_B$. The regression of $[\partial(f_c^2)/\partial\phi]_B$ on $[f_c^2]_B$ has the equation

$$[\partial(f_c^2)/\partial\phi]_B = 0{\cdot}033\,[f_c^2]_B - 0{\cdot}61 \qquad (6)$$

and the correlation coefficient between the two quantities is 0·94. Nelson (1968) found a similar relationship between the total columnar electron content above

Sydney (150° E., 34° S.) and its north–south gradient. However, Nelson's interpretation of the data led him to propose that the gradient in total electron content varies as the square of total content. Inspection of his Fig. 1 suggests that a linear relationship would fit the experimental points better. Thus the north–south gradients in both the total content and the maximum electron density appear to be proportional to their respective quantities.

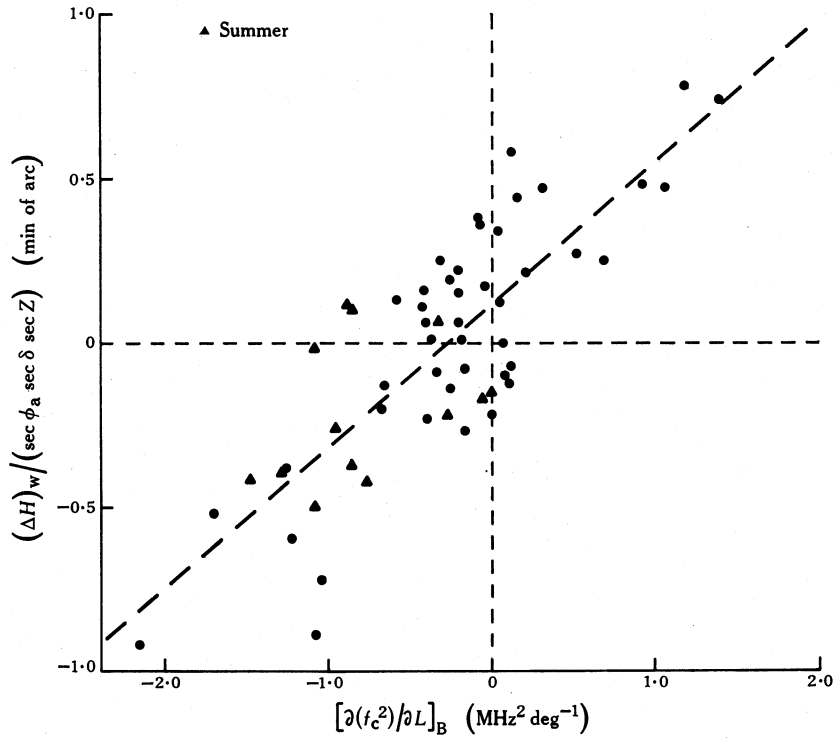

Fig. 5. Correlation diagram showing the dependence of the normalized refraction in hour angle, $(\Delta H)_w/(\sec\phi_a \sec\delta \sec Z)$, on the east–west gradient of the square of the critical frequency for Brisbane. Positive values of $(\Delta H)_w$ and $\partial(f_c^2)/\partial L$ indicate the refraction and the gradient of electron density directed towards the west. The summer measurements (triangles) demonstrate that the electron density gradient has a component directed towards the east on most summer nights. The regression line has the equation

$$(\Delta H)_w/(\sec\phi_a \sec\delta \sec Z) = 0{\cdot}43\,[\partial(f_c^2)/\partial L]_B + 0{\cdot}12.$$

The comparison of the radio measurements of ΔH with the ionospheric measurements was made first, since ΔH is not complicated by the inclusion of the spherical component; because of this, the results for ΔH in the four declination zones, each divided by the normalizing factor $\sec\phi_a \sec\delta \sec Z$, could be combined to provide one average value of ΔH for each of the 56 4-h intervals. A plot of these ΔH against the corresponding measurements of $[\partial(f_c^2)/\partial L]_B$ is given in Fig. 5, which shows a systematic relationship between the two quantities of the kind predicted by equation (5). The slope of the regression line of $\Delta H/(\sec\phi_a \sec\delta \sec Z)$ on $[\partial(f_c^2)/\partial L]_B$ leads via equation (5) to an estimate of the equivalent thickness of the F_2 region, $\tau = 192 \pm 19$ km, where the standard error is quoted.

The radio measurements of $\Delta\delta$ can now be used in conjunction with this estimate of the thickness parameter to separate the two components of declination refraction $(\Delta\delta)_w$ and $(\Delta\delta)_s$. Using equation (3) with $\tau = 192$ km, we compute the spherical component $(\Delta\delta)_s$ for each measurement of $\Delta\delta$, which is then corrected to provide the 'observed' wedge component $(\Delta\delta)_w$. The $(\Delta\delta)_w$ values in all declination zones, each divided by the normalizing factor $\sec^2 Z$, are then combined to provide one

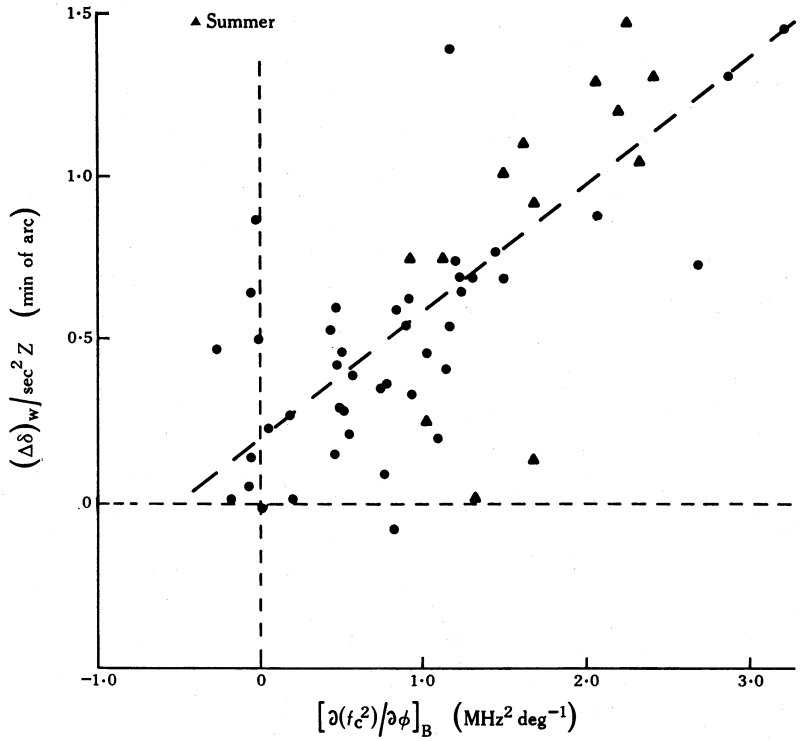

Fig. 6. Correlation diagram showing the dependence of the normalized wedge component of refraction in declination, $(\Delta\delta)_w/\sec^2 Z$, on the north–south gradient of the square of the critical frequency for Brisbane. Positive values of $(\Delta\delta)_w$ and $\partial(f_c^2)/\partial\phi$ indicate the refraction and the gradient of electron density directed towards the north. The summer measurements (triangles) demonstrate that the electron density gradients are higher on most summer nights. The regression line has the equation

$$(\Delta\delta)_w/\sec^2 Z = 0{\cdot}39\,[\partial(f_c^2)/\partial\phi]_B + 0{\cdot}19\,.$$

average value of $(\Delta\delta)_w$ for each of the 56 4-h intervals. The correction for the spherical component is important for only those measurements in the most northerly zone of declination (comprising $\sim\frac{1}{5}$ of the total), so that these averaged determinations of $(\Delta\delta)_w$ are not highly dependent on the value of the thickness parameter which was used for the corrections. A plot of the resulting $(\Delta\delta)_w$ against the corresponding measurements of $[\partial(f_c^2)/\partial\phi]_B$ is given in Fig. 6, which shows a systematic relationship of the kind predicted by equation (2). The slope of the regression line of $(\Delta\delta)_w/\sec^2 Z$ on $\partial(f_c^2)/\partial\phi$ leads via equation (2) to a second estimate of the thickness parameter, $\tau = 172 \pm 24$ km.

Table 4. Determinations of equivalent thickness at Culgoora

Type of measurement	No. of measurements	Equiv. thickness τ (km)	Remarks
$(\Delta H)_w$	56[A]	192 ± 19	No corrections for $(\Delta\delta)_s$
$(\Delta\delta)_w$	56[A]	172 ± 24	Unimportant corrections for $(\Delta\delta)_s$
$(\Delta H)_w + (\Delta\delta)_w$	112[A]	190 ± 12	Unimportant corrections for $(\Delta\delta)_s$
$(\Delta\delta)_s$	43[B]	218 ± 49	Dependent on theoretical corrections for $(\Delta\delta)_w$

[A] Each measurement is an average of ~30 independent determinations of refraction.
[B] Each measurement is an average of ~7 independent determinations of refraction from sources in the declination range $15° < \delta < 35°$.

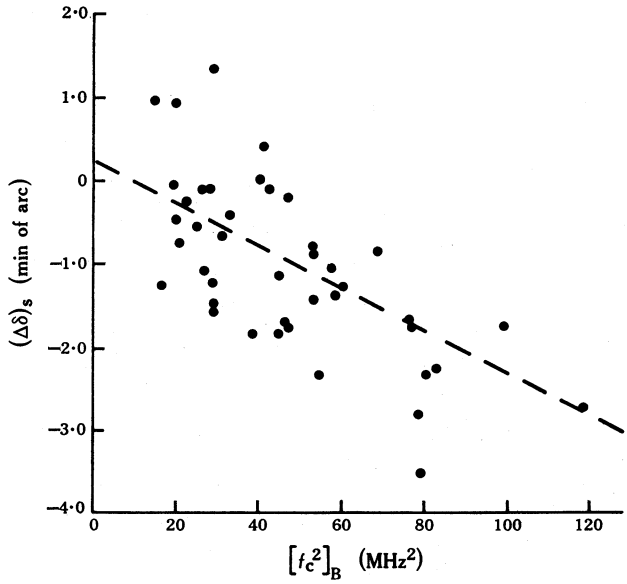

Fig. 7. Correlation diagram showing the dependence of the spherical component of refraction in declination, $(\Delta\delta)_s$, on the square of the critical frequency for Brisbane. Positive values of $(\Delta\delta)_s$ indicate refraction to the north. The regression line has the equation

$$(\Delta\delta)_s = -0{\cdot}025\,[f_c^2]_B + 0{\cdot}24.$$

Since these two largely independent estimates of the equivalent thickness agree to well within the sum of the individual standard errors, it is possible to obtain a more accurate estimate by combining the measurements of $(\Delta H)_w$, $\partial(f_c^2)/\partial L$ and $(\Delta\delta)_w$, $\partial(f_c^2)/\partial\phi$. The regression line of the combined values of normalized refraction on the combined gradients in the square of the critical frequency gives $\tau = 190 \pm 12$ km. Table 4 lists the details of these determinations.

Finally, we have used equation (2) with $\tau = 190$ km to compute the theoretical $(\Delta\delta)_w$ for those observations in the declination range $15° < \delta < 35°$ ($45° < Z < 65°$). The theoretical $(\Delta\delta)_w$ were then subtracted from the observed values of $\Delta\delta$ to give the 'observed' spherical component $(\Delta\delta)_s$. The observed spherical refraction is plotted as a function of $[f_c^2]_B$ in Fig. 7; the scatter is large because the measurements

were derived from relatively few observations ($\sim\frac{1}{5}$ of the total number) at large zenith angles where the irregular refraction is strongest.

The slope of the regression line of $(\Delta\delta)_s$ on $[f_c^2]_B$ in Fig. 7 gives via equation (3) a value for the thickness parameter of $\tau = 218 \pm 49$ km. This derivation of the equivalent thickness is, of course, directly dependent on the value of τ used in evaluating the corrections to the observed $\Delta\delta$ and so cannot be considered an independent estimate. However, the fact that the value of τ derived in this manner is fully consistent with the estimate of τ from the wedge refraction provides good evidence that equation (3) can be used with some confidence to describe the spherical refraction.

Table 5. Measurements of nocturnal equivalent thickness

Reference	Observing interval	Geomag. lat.	Av. $S_{10.7}$[A] (10^{-22} W m^{-2} Hz^{-1})	Av. τ (km)
Jones (1967)	Oct. 1964 – Nov. 1965	−35°·8	75	196
Nelson (1968)	Oct. 1964 – Apr. 1966	−42 ·5	80	219
Titheridge (1973)	June 1965 – Jan. 1966	−38 ·2	78	250–400[B]
Titheridge (1973)	Jan. 1968 – Dec. 1970	−38 ·2	152	260
Present paper	Nov. 1967 – Feb. 1971	−35 ·8	165	187 ± 17
Present paper	Mar. 1971 – Dec. 1971	−35 ·8	117	215 ± 25

[A] Average level of 10·7 cm solar flux.
[B] Summer average ~250 km, winter average ~400 km.

6. Comparisons with Other Measurements and Discussion

Table 5 compares our measurements of equivalent thickness with a representative sample of satellite determinations made by means of Faraday rotation techniques in the past decade. Measurements in the topside ionosphere with satellite-borne probes and ionosondes (see e.g. Reddy *et al.* 1967) and satellite-drag experiments (Jacchia and Slowey 1968) have shown that ion densities and temperatures in the F_2 region depend upon the latitude of the sub-ionospheric point and the intensity of solar u.v. radiation. Accordingly, we have included in Table 5 only those measurements of the thickness parameter made from sites with similar southern geomagnetic latitudes. The flux of solar u.v. radiation during each experiment is indicated by tabulating the average level of the 10·7 cm solar flux. Nocturnal and seasonal influences are virtually suppressed by averaging over 12 h and ~12 months or longer.

First, from the observations of Jones (1967), Nelson (1968) and the present data, all from eastern Australia, it is clear that, despite a wide range in solar activity, the equivalent heights are in good agreement; subdividing our own results into two sections applicable to moderate and high values of solar flux, we find that it is again apparent that the solar activity cycle has no significant effect on the equivalent thickness. This apparent lack of solar control over the vertical distribution of electrons in the ionosphere was also noted by Walker (1971) and Walker and Ting (1972) from Faraday rotation measurements at a lower latitude site in the northern hemisphere. These are unexpected results, since satellite-drag studies by Jacchia and Slowey (1968) and incoherent-scatter observations by Waldteufel and Cogger (1971) show that the neutral gas temperature, which should determine the scale height of the ionizable gas in the ionosphere, increased by ~40% over the interval occupied by these observations.

The measurements of Titheridge (1973) shown in Table 5 apply to a similar southern latitude $\sim 25°$ further east and show a similar lack of solar control over the nocturnal thickness parameter. These values of equivalent thickness are significantly greater than the other measurements in Table 5; the discrepancy is particularly significant in the winter of 1965, where Nelson (1968) finds an average thickness of ~ 220 km while Titheridge measures ~ 400 km. It therefore appears that there can be pronounced longitudinal changes in the factors which influence the shape of the F layer over distances of only a few thousand kilometres.

The lack of correlation between the equivalent thickness and the F_2 gas temperature implies that the vertical distribution of ionization is not completely dependent on the processes of recombination and diffusion (see e.g. Rishbeth and Garriott 1969). A similar conclusion was reached by Furman and Prasad (1973), who used incoherent scatter and ionosonde measurements simultaneously to deduce the equivalent thickness and temperature of the F_2 region. Their results suggested that departure from diffusive equilibrium due to vertical drifts was an important factor in determining the shape of the layer. Titheridge (1973) has suggested that the unexpectedly large values of thickness observed by him during winter nights in 1965 were due to a marked lowering of the O^+/H^+ transition height, although it is not apparent why similar results were not obtained by Nelson (1968) only 3000 km away. It is clear that, until the factors which collectively control the height distribution of ionization are better defined, measurements of equivalent thickness cannot be regarded as accurate indicators of the F_2 gas temperature.

Acknowledgments

The authors wish to thank Mr C. S. Higgins and Miss K. Terrens for their invaluable assistance with the observations and reductions, and the resident staff at the Culgoora Observatory for their cooperation in maintaining the radio equipment at a high state of efficiency.

References

Furman, D. R., and Prasad, S. S. (1973). *J. Geophys. Res.* **78**, 5837.
Jacchia, L. G., and Slowey, J. (1968). *Planet. Space Sci.* **16**, 509.
Jones, K. L. (1967). *Planet. Space Sci.* **15**, 295.
Komesaroff, M. M. (1960). *Aust. J. Phys.* **13**, 153.
Nelson, G. J. (1968). *J. Atmos. Terr. Phys.* **30**, 513.
Payne-Scott, R., and McCready, L. L. (1948). *Terr. Magn.* **53**, 429.
Ratcliffe, J. A., and Weekes, K. (1960). *In* 'Physics of the Upper Atmosphere' (Ed. J. A. Ratcliffe), p. 431 (Academic: New York).
Reddy, B. M., Brace, L. H., and Findlay, J. A. (1967). *J. Geophys. Res.* **72**, 2709.
Rishbeth, H., and Garriott, O. K. (1969). 'Introduction to Ionospheric Physics', International Geophysics Series, Vol. 14 (Academic: New York).
Slee, O. B., and Higgins, C. S. (1973). *Aust. J. Phys. Astrophys. Suppl.* No. 27.
Smerd, S. F., and Slee, O. B. (1966). *Aust. J. Phys.* **19**, 427.
Smith, F. G. (1952). *J. Atmos. Terr. Phys.* **2**, 350.
Titheridge, J. E. (1973). *Planet. Space Sci.* **21**, 1775.
Waldteufel, P., and Cogger, L. (1971). *J. Geophys. Res.* **76**, 5322.
Walker, G. O. (1971). *J. Atmos. Terr. Phys.* **33**, 1041.
Walker, G. O., and Ting, S. D. (1972). *J. Atmos. Terr. Phys.* **34**, 283.

Manuscript received 17 May 1974